

# An improved strength-measurement technique for brittle materials

M J Matthewson and J E Field

Physics and Chemistry of Solids, Cavendish Laboratory,  
Madingley Road, Cambridge CB3 0HE, UK

Received 20 September 1979

**Abstract** An improved apparatus for determining the fracture strength of brittle materials by a hydraulic bursting technique is described. The new design greatly reduces the number of specimens which fail at their edge and reduces the scatter in the results. To complement this, a more detailed theory is developed to analyse results. An investigation of the strength of silicon nitride as a function of the impact velocity of a water jet illustrates the use of the apparatus. A method for converting fracture stress data to equivalent flaw size data is given which allows a more physically meaningful and useful presentation of results.

## 1 Introduction

In recent years there has been a growing interest in assessing impact, wear and indentation damage to a specimen in terms of strength loss or flaw growth. Gorham and Rickerby (1975) described a strength test apparatus in which a circular disc specimen is supported near its edge and is burst by hydraulic pressure applied to one side. The fracture stress may be calculated from the bursting pressure. Their paper discusses the advantages this technique has over other methods which are available; in particular, the fraction of specimens which fail at the support or the edge is comparatively low. While the Gorham and Rickerby apparatus has a relatively low frequency of edge failures, Rickerby (1977) has found that for 25 mm radius glass discs edge failures are not insignificant: some 15% of 3 mm thick and 25% of 6 mm thick specimens fail in this way. Our work with this test shows that failures of this sort occur at the support, rather than the edge, and are due to a large tensile circumferential stress component (equal to about one-half the stress at the centre of the disc) interacting with local stress concentrations caused by support irregularities. Figure 1 illustrates specimens which failed (a) at the support and (b) away from the support.

The hydraulic test approach has already provided useful results in assessing impact damage and erosion parameters of a variety of brittle materials (Field *et al* 1974, 1979a, 1979b, Rickerby 1977). Specimens of some materials are often in short supply and extremely costly and wasting a proportion of them by support failure is undesirable. The motivation for the present work was to reduce the problem of support failures.

This paper describes a modified hydraulic tester where the support ring radius is reduced giving an acceptably low

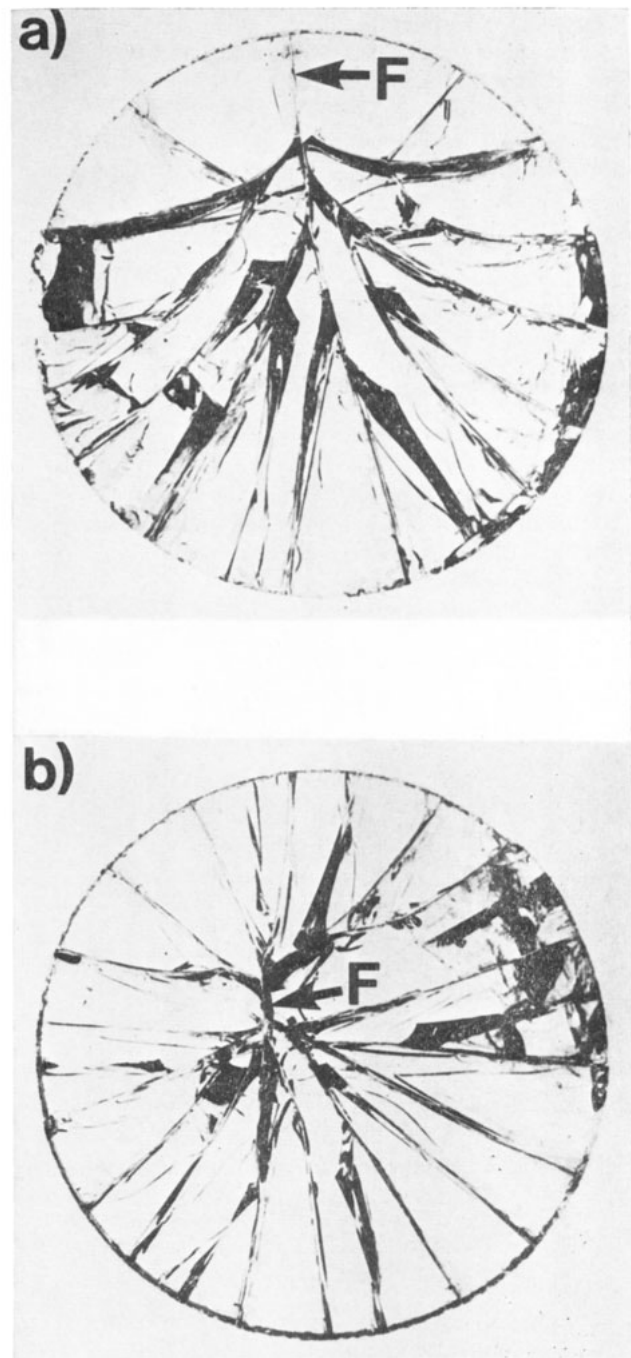


**Figure 1** Glass discs (25 mm radius) broken in the hydraulic tester. Failure initiated at points *F*, (a) at the support and (b) away from the support where the stress field is well defined.

frequency of support failures. The stress distributions across the disc which have been used previously are not accurate in this situation and a new distribution is derived theoretically. The use of the new apparatus is illustrated by measurements of the strength of silicon nitride discs after impact by water jets. These results are then interpreted in terms of equivalent induced flaw sizes which are physically more meaningful.

The notation used in this paper is given below.

- $r_2$  radius of disc specimen
- $r_1$  radius of support ring
- $t$  disc thickness
- $E$  Young's modulus of disc material

- $\nu$  Poisson ratio of disc material
- $q(r)$  radial distribution of pressure (equal to  $P$ , the uniform applied pressure)
- $w(r)$  radial distribution of displacement of the disc
- $\sigma_r(r)$  radial stress component at the surface of the disc
- $\sigma_\theta(r)$  circumferential stress component at the surface of the disc
- $\phi$  angle between radius vector and fracture origin
- $\sigma_f$  fracture stress
- $\rho = r_2/r_1$
- $\xi = r/r_1$
- $D' = \frac{Et^3}{12(1-\nu^2)}$

**2 Hydraulic test apparatus**

**2.1 Theory**

A scale schematic diagram of the apparatus is shown in figure 2. The specimen of radius  $r_2$  is supported by a ring of radius  $r_1$  and a uniform pressure is exerted on the disc, via a neoprene

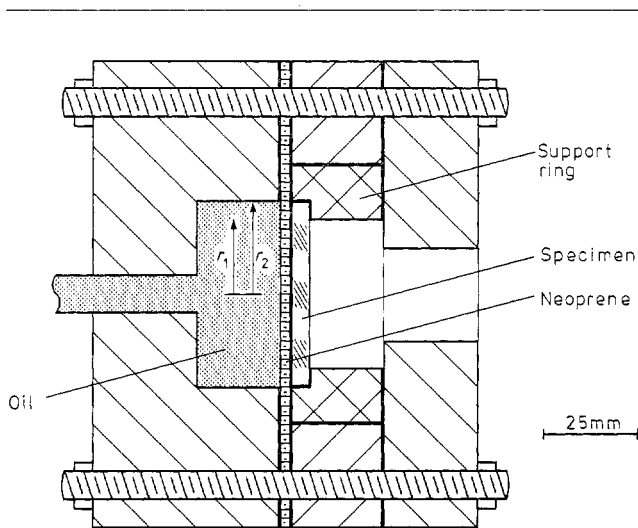


**Figure 2** Scale diagram of the hydraulic strength test apparatus.

diaphragm, by a hydraulic system. Gorham and Rickerby used values of  $r_2 = 25$  mm and  $r_1 = 23$  mm. The stress distribution for a disc simply supported at its edge is given by Timoshenko (1940) and is fairly accurate in this case. Mansfield (1963) gives a more appropriate distribution which allows for the stiffening effect of the overhang of the disc over the support, but does not account for the pressure applied to the overhang.

Timoshenko (1940) gives the differential equation for the displacements,  $w(r)$ , of a thin circular plate under an axially symmetric pressure distribution,  $q(r)$ :

$$\frac{1}{r} \frac{d}{dr} \left\{ r \frac{d}{dr} \left[ \frac{1}{r} \frac{d}{dr} \left( r \frac{d}{dr} w(r) \right) \right] \right\} = \frac{q(r)}{D'} \quad (1)$$

In this case  $q(r) = P$ , the uniform applied pressure, giving a general solution to (1):

$$w(r) = \frac{Pr_1^4}{64D'} \{ A + B \ln(r/r_1) + C(r/r_1)^2 + D(r/r_1)^2 \ln(r/r_1) + (r/r_1)^4 \} \quad (2)$$

Two sets of values for the coefficients  $A$ ,  $B$ ,  $C$  and  $D$  may be found corresponding to the solutions for  $r > r_1$  and  $r < r_1$

by using the boundary conditions given by Mansfield (1963). From the results the stress distribution on the surface of the disc may be found.

$$\sigma_r = \frac{3Pr_1^2}{8t^2} \{ \rho^2[3\nu + 1 - 4(1 + \nu) \ln(\rho)] + 2(1 - \nu) - (3 + \nu)\xi^2 \}$$

and (3)

$$\sigma_\theta = \frac{3Pr_1^2}{8t^2} \{ \rho^2[3\nu + 1 - 4(1 + \nu) \ln(\rho)] + 2(1 - \nu) - (1 + 3\nu)\xi^2 \}$$

for  $r < r_1$ . These equations reduce to those of Timoshenko when  $r_1 = r_2$ .

Figure 3 shows the radial distribution of these stresses for various values of  $r_1/r_2$ . The stresses are normalised to the central stress when  $r_1/r_2 = 1$ : effectively they are the stress distributions for a fixed applied pressure but differing support

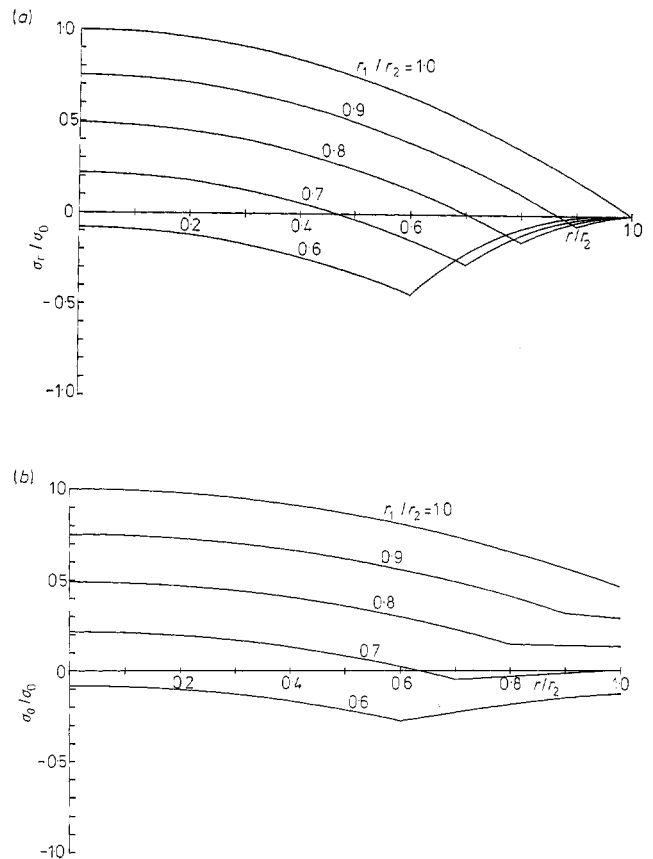


**Figure 3** Radial distribution of (a)  $\sigma_r$  and (b)  $\sigma_\theta$  for various values of  $r_1/r_2$  each normalised to the central value when  $r_1 = r_2$  ( $\sigma_0$ ).

ring radii. As  $r_1/r_2$  decreases, the magnitude of the circumferential stress at the support decreases with respect to the central stress, decreasing the probability of a support failure. However, the central stress also decreases with  $r_1/r_2$ . This implies that to reach a certain stress level at the centre of the disc, the hydrostatic pressure must be increased as  $r_1/r_2$  decreases. Hence, as  $r_1/r_2$  decreases, the contact pressure at the support increases if a fixed central stress is to be obtained. If  $r_1/r_2$  is near unity the circumferential stress component is large but if  $r_1/r_2$  is small a large contact pressure results. In

order to minimise the number of support failures a compromise value for  $r_1/r_2$  must be chosen and a value of 0.8 has been found to be suitable. This gives a reduction in the circumferential stress component of about 30% with respect to support at the edge, although the contact pressures are doubled. The circumferential stress is more important than the contact pressure, as the overall effect is found experimentally to reduce the number of support failures. Experiments on 6 mm thick glass discs show that with  $r_2 = 25$  mm and  $r_1 = 20$  mm 5% fail at the support compared with 25% for  $r_1 = 23$  mm. At this level support failures may be safely ignored.

Timoshenko gives a correction term which should be added to the displacements,  $w(r)$ , which takes into account the effect of shear within the plate and the lateral extension due to the applied pressure. Additional tensile stress components  $\Delta\sigma_r$  and  $\Delta\sigma_\theta$  can readily be calculated from the correction term and reduced to:

$$\Delta\sigma_r = \Delta\sigma_\theta = \frac{(3 + \nu)}{4(1 - \nu)} P. \quad (4)$$

The fracture stress  $\sigma_f$  may be calculated using

$$\sigma_f = \sigma_r \sin^2 \phi + \sigma_\theta \cos^2 \phi$$

where  $P$  takes the value of the bursting pressure,  $r$  is the distance between the fracture origin and the centre of the disc and  $\phi$  is the angle between the fracture origin and the radius vector.

### 2.2 Experimental

The theoretically derived stress distribution has been verified experimentally. Strain gauges (Showa type N22-FA-2 double element resistance gauges) were attached to 3 mm and 6 mm glass discs at various distances from the centre (0, 8 and 16 mm). The discs were loaded in the tester and the strain gauge output was found as a function of applied pressure. From the results the function  $\epsilon/P$ , where  $\epsilon$  is the strain, is calculated by linear regression.

Figure 4 compares the experimental and theoretical determinations of the strain distribution across the specimens for both disc thicknesses. The theoretical curves are calculated using equations (3) and (4) and using

$$\begin{aligned} \epsilon_r &= \frac{1}{E} (\sigma_r - \nu\sigma_\theta) \\ \epsilon_\theta &= \frac{1}{E} (\sigma_\theta - \nu\sigma_r). \end{aligned} \quad (5)$$

Equations (5) are derived from the elasticity equations, given that the stress perpendicular to the surface,  $\sigma_z$ , is zero. The values of elastic constants are  $E = 69$  GPa and  $\nu = 0.25$  (Woodward 1974). The horizontal error bars are due to uncertainty in positioning the gauges and also that the gauges are of finite size (2 mm) and average the strains over their length. The vertical error bars are estimates of the scatter in the slopes of  $\epsilon$  against  $P$  plots.

For the 3 mm discs (figure 4(a)) the theory fits the measured circumferential strains very well. However, for the radial strains, the fit is good everywhere except near the support ring where the measured strain is about 200% larger than is predicted theoretically. This can be attributed to the stress field due to the line loading at the support interacting with the stress field due to the plate bending. However, this discrepancy is not significant as the great majority of specimens fail near the centre of the disc where there is excellent correlation between theory and experiment.

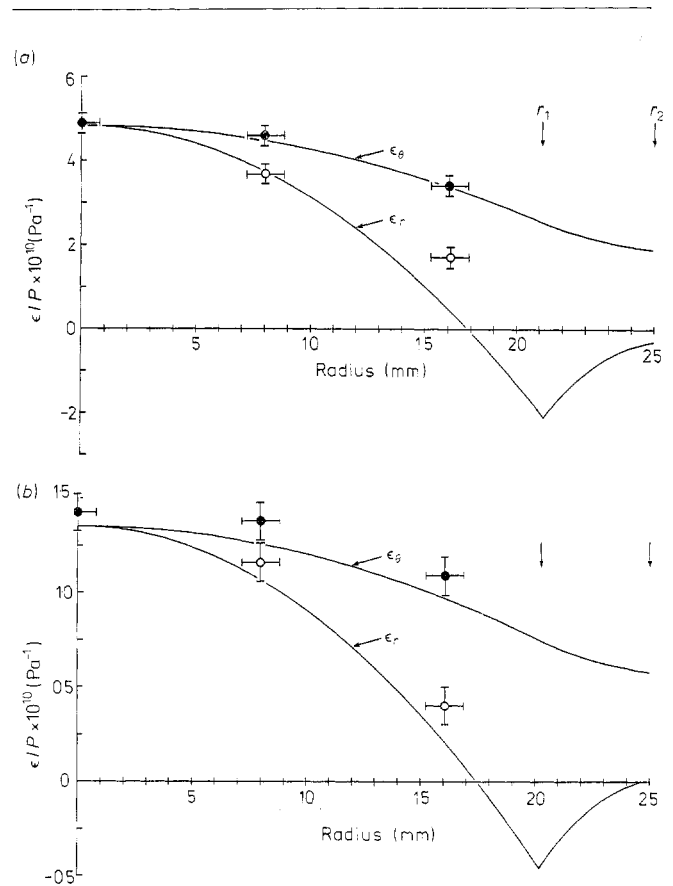


Figure 4 Comparison between theory and experiment for the strain distribution (divided by the pressure) across (a) 3 mm thick and (b) 6 mm thick discs. ○, radial component; ●, circumferential component.

For the 6 mm discs (figure 4(b)) the experimental points lie close to the theory line although they are systematically slightly higher. This error is due to a combination of factors. Firstly, the theory assumes that the thickness is small compared with the width and this is not strictly valid for  $r_1 = 20$  mm and  $t = 6$  mm. A full treatment for a thick plate is more complex and has been left for future work. Secondly, deviations caused by stresses at the support are more significant as a greater pressure is needed to generate the same stresses at the centre of a thicker specimen.

### 3 The residual strength of silicon nitride

The pressure tester has been used in the past to examine the variation of strength of various materials with the velocity of impacting water jets. The results have application to the studies of rain erosion since the pressure tester technique provides a rapid and inexpensive method of evaluating erosion resistance quantitatively. The impact behaviour of infrared transparent materials has received much attention in recent years (Field *et al* 1974, 1979a, 1979b) and the results of an investigation on hot-pressed silicon nitride (supplied by FMI) are presented here. This type of material is expensive and in short supply. Forty-five specimens were available for this investigation and consequently wastage of specimens was undesirable. With the modified pressure tester no support failures occurred and each specimen yielded useful information.

The results presented here outline an experimental programme for obtaining data on the impact properties of a material using the pressure tester and other techniques. The

methods illustrate not only the use of the tester, but also how the performance of materials may be rapidly evaluated in a quantitative manner. The results can then be used to determine how improvements can be made to material properties.

The silicon nitride discs were impacted centrally by water jets of 3 mm diameter produced by an apparatus which is described fully elsewhere by Bowden and Brunton (1961) and Field *et al* (1979a). The discs were then burst in the tester with the impacted surfaces in tension. Parameters used for calculating results are  $r_1=20$  mm,  $r_2=25$  mm,  $t=3$  mm and  $\nu=0.27$ . Figure 5 shows the results of the fracture stress plotted as a function of jet velocity. Each data point is an average for five specimens. Up to a velocity of 400 m s<sup>-1</sup> the residual strength remains constant at its unimpacted value.

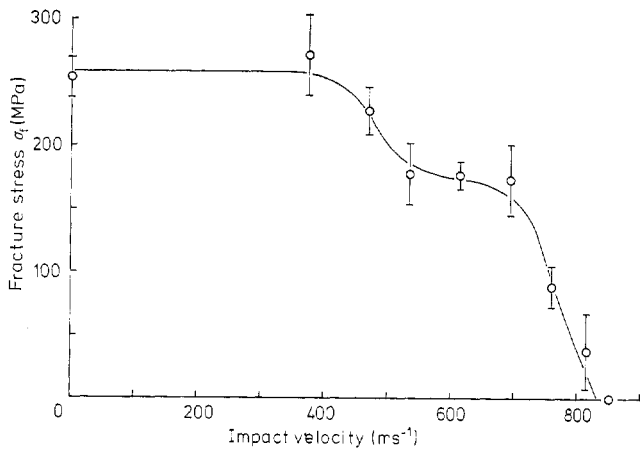


Figure 5 Fracture stress of hot-pressed silicon nitride as a function of impact velocity for impacts by 3 mm diameter water jets.

The strength then falls to a constant value between 500 and 700 m s<sup>-1</sup>. This fall is due to the formation of small circumferential cracks around the impact site by the Rayleigh surface wave (Bowden and Field 1964, Field *et al* 1979a). Above 700 m s<sup>-1</sup> the residual strength falls towards zero due to the formation of long radial cracks in the specimen until at about 850 m s<sup>-1</sup> the discs are fragmented by the impact. The form of the residual strength curve is well understood and is described elsewhere (e.g. Field *et al* 1979b).

Expressing residual strength characteristics in terms of fracture stresses is not a particularly useful way of representing the results as fracture stresses depend not only on fundamental material properties, but also on the ambient environment, the loading system and the loading rate. For this reason, the results are converted to the equivalent flaw sizes which are induced by the impact. When the data are presented in this form the fracture stress may be calculated for any loading condition or environment. In general the flaw sizes may be calculated from the fracture stresses using

$$c = \frac{1}{\alpha} \left( \frac{\sigma_f}{K_{IC}} \right)^2$$

where  $c$  is a measure of the flaw size,  $K_{IC}$  is the critical stress intensity factor and  $\alpha$  is a constant depending on the geometries of the flaw and specimen. The flaws are observed to be of the order of millimetres in length in the surface and are therefore not small compared to the specimen thickness

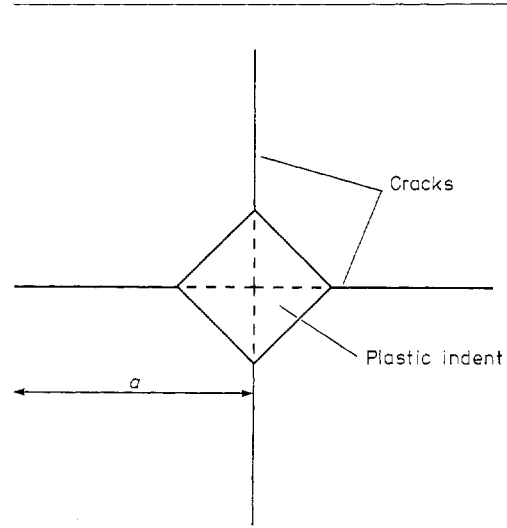


Figure 6 Schematic diagram showing the pit formed by plastic deformation and radial cracks produced by Vickers indentation.

(3 mm). Therefore the flaw may be modelled by a slot crack of length  $2c$  in the surface: in this case  $\alpha$  has the value  $\pi$ .

The critical stress intensity factor,  $K_{IC}$ , is measured using the indentation technique of Lawn and Fuller (1975) in which a Vickers indenter is loaded on to the specimen until radial cracks form. Figure 6 shows these cracks schematically.  $K_{IC}$  is given by

$$K_{IC} = \frac{\chi L}{a^{3/2}}; \quad \chi = \frac{1}{\pi^{3/2} \tan \psi}$$

where  $L$  is the applied load and  $\psi$  is the indenter semi-angle and  $a$  is the length of the radial cracks. Figure 7 shows typical results of  $a^{3/2}/\chi$  as a function of  $L$  giving a value of  $K_{IC} = 4.9 \pm 0.3 \text{ MNm}^{-3/2}$ . Results for several specimens give a mean value of  $K_{IC} = 5.2 \pm 0.3 \text{ MNm}^{-3/2}$ . This result agrees well with a value of  $4.9 \text{ MNm}^{-3/2}$  obtained by Evans (1978, private communication) on the same material using a double cantilever method.

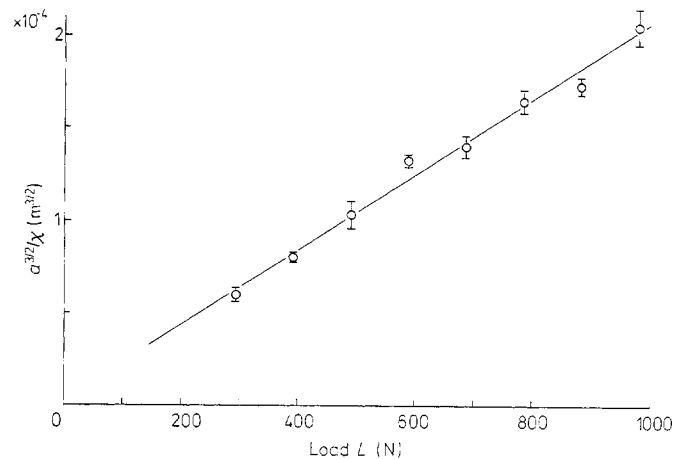
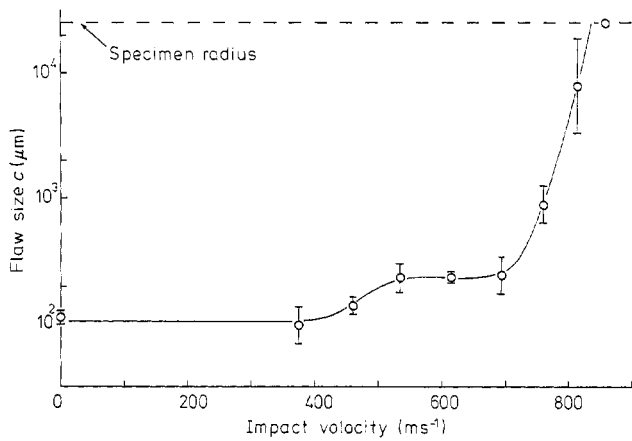


Figure 7 Typical results of plotting  $a^{3/2}/\chi$  against  $L$ . The inverse of the slope gives  $K_{IC} = 4.9 \text{ MNm}^{-3/2}$ .



**Figure 8** Fracture stress data of figure 5 replotted in terms of the equivalent flaw size,  $c$ .

Figure 8 shows the flaw size,  $c$ , induced by the impact as a function of impact velocity. For unimpacted specimens  $c = 110 \pm 10 \mu\text{m}$ . The material is granular in nature with grains of the order of  $10 \mu\text{m}$  in diameter and the intrinsic flaws are therefore much larger than the grains. By adjustment of the manufacturing process it should be possible to decrease the flaw sizes to of the order of the grain size thus increasing the strength of the material. This would also have the effect of increasing the damage threshold velocity ( $400 \text{ m s}^{-1}$ ) as this is a function of the intrinsic flaw size (Field *et al* 1979b).

#### 4 Conclusions

The advantages of the hydraulic test apparatus are (i) the circularly symmetric stress field, (ii) the large proportion of specimen surface tested, (iii) the ease and rapidity of operation, and (iv) the possibility of miniaturisation; we have used specimens down to 25 mm in diameter.

The improvement to the pressure tester has reduced the number of specimens which fail at the support to an insignificant level. The technique has now been developed to the stage where results are accurate and reliable enough for the tester to be used commercially as a rapid and inexpensive method for evaluation and quality control of materials.

The use of the tester is illustrated by an investigation of the post-impact strength properties of a hot-pressed silicon nitride in which the features of the modified design result in accurate and reliable data. The fracture stress data have been converted to equivalent flaw size data which is more physically meaningful and has enabled a suggestion for improving the material to be made.

#### Acknowledgments

We thank the Ministry of Defence (Procurement Executive) for financial support during the course of this research. One of us (MJM) also thanks the SRC and Churchill College, Cambridge.

#### References

- Bowden F P and Brunton J H 1961 The deformation of solids by liquid impact at supersonic speeds  
*Proc. R. Soc. A* **263** 433–50
- Bowden F P and Field J E 1964 The brittle fracture of solids by liquid impact, by solid impact, and by shock  
*Proc. R. Soc. A* **282** 331–52

Field J E, Camus J-J, Gorham D A and Rickerby D G 1974 Impact damage produced by large water drops  
*Proc. 4th Int. Conf. on Rain Erosion and Allied Phenomena, Meersburg*, pp 395–420 (Farnborough: RAF)

Field J E, Gorham D A, Hagan J T, Matthewson M J, Swain M V and Van Der Zwaag S 1979a Liquid jet impact and damage assessment for brittle solids  
*Proc. 5th Int. Conf. on Erosion by Liquid and Solid Impact, Cambridge*

Field J E, Gorham D A and Rickerby D G 1979b High speed liquid jet and drop impact on brittle materials  
*Erosion: Prevention and Useful Applications*, ASTM, STP 664, ed. W F Adler pp 298–319

Gorham D A and Rickerby D G 1975 A hydraulic strength test for brittle materials  
*J. Phys. E: Sci. Instrum.* **8** 794–6

Lawn B R and Fuller E R 1975 Equilibrium penny-like cracks in indentation fracture  
*J. Mater. Sci.* **10** 2016–24

Mansfield E H 1963 The stiffening effect of an overhang in a circular plate  
*J. R. Aero. Soc.* **67** 671–2

Rickerby D G 1977 High velocity liquid impact and fracture phenomena  
*PhD Thesis, University of Cambridge, UK*

Timoshenko S 1940 *Theory of Plates and Shells* (New York: McGraw-Hill)

Woodward A D 1974 Crack propagation in glasses  
*PhD Thesis, University of Cambridge, UK*